

## CURRENT SIGNS OF DYNAMICAL DARK ENERGY

JOAN SOLÀ PERACAU<sup>1,2</sup>, ADRIÀ GÓMEZ-VALENT<sup>1,2</sup>, JAVIER DE CRUZ PÉREZ<sup>1,2</sup>  
*Draft version November 9, 2018*

### ABSTRACT

Investigations on dark energy (DE) are currently inconclusive about its time evolution. Hints of this possibility do glow now and then in the horizon. Depending on the datasets used and the methodology employed one may reach different levels of evidence or no evidence at all. Herein we assess the current status of dynamical dark energy (DDE) in the light of a large body of updated SNIa+ $H(z)$ +BAO+LSS+CMB observations, using the full CMB likelihood. The performance of the  $\Lambda$ CDM model (with equation of state  $w = -1$  for  $\Lambda$ ) is confronted with that of the general XCDM and CPL parametrizations, as well as with the traditional  $\phi$ CDM model based on the scalar field potential  $V \sim \phi^{-\alpha}$ . In particular, we gauge the impact of the bispectrum in the LSS and BAO parts, and show that the subset of CMB+BAO+LSS observations may contain the bulk of the DDE signal. The departure from  $w = -1$  is significant: roughly  $2.6\sigma$  for XCDM and  $2.9\sigma$  for  $\phi$ CDM. In both cases the full Bayesian evidence for DDE is found to be positive even for a prior range extending over several standard deviations from the mean when the bispectrum is taken into account. We report also on positive signs from the preliminary results of Planck 2018 data using the compressed CMB likelihood.

*Subject headings:* cosmological parameters — dark energy — large-scale structure of universe

### 1. INTRODUCTION

Even if the existence proof of the DE is not iron-clad, the great majority of cosmologists are agreed that the universe is in accelerated expansion (Riess et al., Perlmutter et al. 1998,1999; Planck Collab. 2015) and that some physical cause must be responsible for it. The canonical picture in GR is to assume that such cause is the presence of a cosmological constant (CC) term,  $\Lambda$ , in Einstein's equations. No reason, however, is given for its constancy throughout the entire cosmic history. In fact,  $\Lambda = \text{const.}$  is not required by the cosmological principle. Such oversimplification might be at the root of the Cosmological Constant Problem, namely the appalling discrepancy between the measured vacuum energy density,  $\rho_\Lambda = \Lambda/(8\pi G) \sim 10^{-47} \text{ GeV}^4$  (G being Newton's constant), and the incommensurably larger value predicted in quantum field theory (QFT) (Weinberg 1989; Peebles & Ratra, Padmanabhan 2003; Solà 2013).

Aside from theoretical problems, a number of persisting tensions with the data (particularly on the local value of the Hubble parameter (Riess et al. 2016,2018a) and the large scale structure formation data (Macaulay et al. 2013)) suggest that the concordance or  $\Lambda$ CDM model, with rigid  $\Lambda$ -term, might be performing insufficiently at the observational level. The possibility to alleviate some of these problems by assuming that  $\rho_\Lambda$ , or in general the DE, might be (slowly) dynamical is a natural option to test, see e.g. Valentino, Melchiorri & Mena (2017). Here we are primarily spurred by these phenomenological considerations and the disparity of different results. For instance, hints of DDE were highlighted in Salvatelli et al. (2014); Solà, Gómez-Valent &

de Cruz Pérez (2015). At the same time, nonparametric studies of the DDE suggest positive evidence at about  $3.5\sigma$  c.l., see Zhao et al. (2017). Such confidence level is actually comparable to that achieved through specific models of DDE, in which attempts were made to cure the mentioned tensions – see e.g. (Solà, Gómez-Valent & de Cruz Pérez 2017a,b) and references therein. Other recent works, however, find milder evidence of DDE or simply no sizeable deviation from the  $\Lambda$ CDM, see Ferreira et al. (2017); Costa et al. (2017); Park & Ratra (2018a,b); Tsiapi & Basilakos (2018), for example. In this Letter, we reassess the situation. The novelty is that we pay due attention to the sensitivity of the DDE signal to potentially relevant features sitting in data such as LSS, BAO and CMB. We try to clarify why some authors find evidence in contrast to others by noting that specific ingredients of the data usually not taken into account (e.g. the inclusion of the bispectrum), may develop more sensitivity to DDE. This fact, if confirmed, could guide us into future strategies helping to consolidate the DDE signal, if it is there.

### 2. DDE PARAMETRIZATIONS AND MODELS

We consider two generic parametrizations of the DDE, together with a specific  $\phi$ CDM model with a quintessence potential and fit them to a large updated set of SNIa+ $H(z)$ +BAO+LSS+CMB observations.

The first of the DDE parametrizations under study is the conventional XCDM (Turner & White 1997). In it both matter and DE are self-conserved (non-interacting) and the DE density is simply given by  $\rho_X(a) = \rho_{X0} a^{-3(1+w_0)}$ , where  $\rho_{X0} = \rho_\Lambda$  is the current value and  $w_0$  the (constant) EoS parameter of the DE fluid. For  $w_0 = -1$  we recover the  $\Lambda$ CDM model with a rigid CC. For  $w_0 \gtrsim -1$  the XCDM mimics quintessence, whereas for  $w_0 \lesssim -1$  it mimics phantom DE. It is worth checking if a dynamical EoS for the DE can furnish a better description of the observational data. So we consider the well-known CPL parametrization (Chevalier &

sola@fqa.ub.edu  
adriagova@fqa.ub.edu  
decruz@fqa.ub.edu

<sup>1</sup> Departament de Física Quàntica i Astrofísica, Universitat de Barcelona, Diagonal 647, E-08028 Barcelona, Catalonia, Spain

<sup>2</sup> Institute of Cosmos Sciences (ICCUB), Universitat de Barcelona, Diagonal 647, E-08028 Barcelona

TABLE 1  
MEAN FIT VALUES AND  $1\sigma$  LIMITS (68.3% C.L.) FOR  $\Lambda$ CDM, XCDM AND  $\phi$ CDM USING DATASET DS1

Model	$H_0$ (km/s/Mpc)	$\omega_{\text{cdm}}$	$\omega_{\text{b}}$	$w_0$	$\alpha$	$\sigma_8(0)$
DS1 with Spectrum (DS1/SP)						
$\Lambda$ CDM	$69.22^{+0.48}_{-0.49}$	$0.1155^{+0.0011}_{-0.0010}$	$0.02247^{+0.00020}_{-0.00019}$	-1	-	$0.813^{+0.008}_{-0.009}$
XCDM	$68.97^{+0.76}_{-0.79}$	$0.1151^{+0.0013}_{-0.0014}$	$0.02251^{+0.00021}_{-0.00020}$	$-0.986^{+0.030}_{-0.029}$	-	$0.811 \pm 0.010$
$\phi$ CDM	$68.70^{+0.66}_{-0.61}$	$0.1147^{+0.0013}_{-0.0012}$	$0.02255^{+0.00020}_{-0.00022}$	-	$< 0.092$	$0.808 \pm 0.010$
DS1 with Bispectrum (DS1/BSP)						
$\Lambda$ CDM	$68.21^{+0.40}_{-0.38}$	$0.1176^{+0.0008}_{-0.0009}$	$0.02231^{+0.00019}_{-0.00018}$	-1	-	$0.804^{+0.007}_{-0.008}$
XCDM	$67.18^{+0.63}_{-0.68}$	$0.1161 \pm 0.0012$	$0.02244^{+0.00021}_{-0.00020}$	$-0.945^{+0.029}_{-0.028}$	-	$0.795^{+0.010}_{-0.009}$
$\phi$ CDM	$67.19^{+0.67}_{-0.64}$	$0.1160^{+0.0013}_{-0.0012}$	$0.02245 \pm 0.00021$	-	$0.150^{+0.070}_{-0.086}$	$0.793 \pm 0.009$

NOTE. — The best-fit values for the considered models using dataset DS1, i.e. all SNIa+ $H(z)$ +BAO+LSS+CMB data, with full Planck 2015 CMB likelihood. In all cases a massive neutrino of 0.06 eV has been included. The first block involves BAO+LSS data using the matter (power) spectrum (SP) and is labelled DS1/SP. The second block includes both spectrum and bispectrum, and is denoted DS1/BSP. See text for more details. We display the fitting results for a few parameters only, among them those that characterize the considered DDE models: the EoS parameter  $w_0$  for XCDM, and the power  $\alpha$  of the potential for  $\phi$ CDM, as well as three conventional ones:  $H_0$  (Hubble parameter),  $\omega_{\text{cdm}} = \Omega_{\text{cdm}}h^2$  and  $\omega_{\text{b}} = \Omega_{\text{b}}h^2$  for cold dark matter and baryons. The remaining three ( $A_s, n_s, \tau$ ) are not quoted. For convenience we also list the computed values of  $\sigma_8(0)$ .

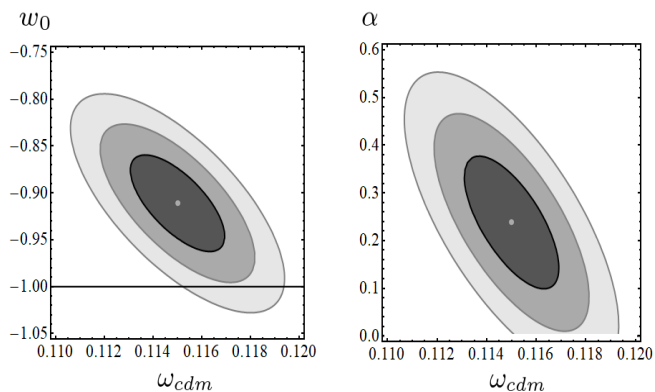


FIG. 1.— Likelihood contours for the XCDM parametrization (left) and the considered  $\phi$ CDM model (right) in the relevant planes ( $\omega_{\text{cdm}}, w_0$ ) and ( $\omega_{\text{cdm}}, \alpha$ ) respectively, after marginalizing over the remaining parameters. Dataset DS2/BSP is used in both cases (cf. first block of Table 2). The various contours correspond to  $1\sigma$ ,  $2\sigma$  and  $3\sigma$  c.l. The central values in both cases are shifted  $> 2.5\sigma$  away from the  $\Lambda$ CDM, i.e. from  $w_0 = -1$  and  $\alpha = 0$  in each case.

Polarski, Linder 2001,2003), which is characterized by the following EoS:

$$w(a) = w_0 + w_1(1 - a) = w_0 + w_1 \frac{z}{1+z}, \quad (1)$$

where  $z = a^{-1} - 1$  is the cosmological redshift. For  $w_0 = -1$  and  $w_1 = 0$ , we recover the concordance model. Let us now explain the theoretical framework of the  $\phi$ CDM studied in this work, which has a well-defined local Lagrangian description. In this kind of models, the DE is described in terms of a scalar field,  $\phi$ , which we take dimensionless. The corresponding expressions for the energy density and pressure read

$$\rho_\phi = \frac{M_P^2}{16\pi} \left( \frac{\dot{\phi}^2}{2} + V(\phi) \right) \quad p_\phi = \frac{M_P^2}{16\pi} \left( \frac{\dot{\phi}^2}{2} - V(\phi) \right). \quad (2)$$

Dots indicate derivatives with respect to the cosmic time and  $M_P = 1/\sqrt{G} = 1.2211 \times 10^{19}$  GeV is the Planck mass in natural units. As a representative potential we borrow the traditional quintessence potential (Peebles & Ratra 1988)

$$V(\phi) = \frac{1}{2} \kappa M_P^2 \phi^{-\alpha}, \quad (3)$$

where  $\kappa$  is a dimensionless parameter. We expect it to be positive since  $\rho_\Lambda > 0$ . In what follows, when referring to the  $\phi$ CDM model we will implicitly assume this form of the potential. The power  $\alpha$  in it should be positive as well, but sufficiently small so that  $V(\phi)$  mimics an approximate CC slowly evolving with time. In our case we take  $\alpha$  as a free parameter while  $\kappa$  is a derived one, as discussed below.

When the cosmic evolution is characterized by the dominant energy density  $\rho(a) \propto a^{-n}$  ( $n = 3$  for the matter-dominated epoch and  $n = 4$  for radiation-dominated), the EoS parameter for  $\phi$  remains constant and can be computed analytically. From (2) and (3) we find:

$$w_\phi = \frac{p_\phi}{\rho_\phi} = -1 + \frac{\alpha n}{3(2 + \alpha)}. \quad (4)$$

However, around the current time (and in the transit from radiation to matter domination) the EoS is dynamical and has to be computed numerically. It follows from solving the corresponding Klein-Gordon equation for  $V(\phi)$  given by (3). We can conveniently write it in terms of the scale factor (prime stands for  $d/da$ ):

$$\phi'' + \left( \frac{H'}{H} + \frac{4}{a} \right) \phi' - \frac{\alpha \kappa M_P^2 \phi^{-(\alpha+1)}}{(aH)^2} = 0. \quad (5)$$

This equation is coupled to the cosmological equations under appropriate initial conditions, which we set at the radiation epoch. By generalizing the procedure of (Solà,

TABLE 2  
MEAN FIT VALUES AND  $1\sigma$  LIMITS (68.3% C.L.) FOR  $\Lambda$ CDM, XCDM AND  $\phi$ CDM USING DATASET DS2

Model	$H_0$ (km/s/Mpc)	$\omega_{\text{cdm}}$	$\omega_{\text{b}}$	$w_0$	$\alpha$	$\sigma_8(0)$
DS2 with Bispectrum (DS2/BSP)						
$\Lambda$ CDM	$68.20^{+0.38}_{-0.41}$	$0.1176^{+0.0008}_{-0.0009}$	$0.02230 \pm 0.00019$	-1	-	$0.805 \pm 0.0007$
XCDM	$66.36^{+0.76}_{-0.86}$	$0.1155^{+0.0014}_{-0.0012}$	$0.02247 \pm 0.00021$	$-0.911^{+0.035}_{-0.034}$	-	$0.788 \pm 0.010$
$\phi$ CDM	$66.45 \pm 0.74$	$0.1154 \pm 0.0013$	$0.02248^{+0.00020}_{-0.00021}$	-	$0.240^{+0.086}_{-0.102}$	$0.789 \pm 0.010$
DS2/BSP with Planck 2018 (compressed likelihood)						
XCDM	$67.08 \pm 0.73$	$0.1191 \pm 0.0008$	$0.02259 \pm 0.00013$	$-0.932 \pm 0.0025$	-	$0.774 \pm 0.013$
$\phi$ CDM	$67.20 \pm 0.70$	$0.1191 \pm 0.0008$	$0.02259 \pm 0.00013$	-	$0.168 \pm 0.068$	$0.773 \pm 0.012$

NOTE. — As in Table 1, but using dataset DS2/BSP, which involves BAO+LSS+CMB data only. In the first block we use the full likelihood for Planck 2015, whereas in the second we use the compressed CMB likelihood for the more recent Planck 2018 data. See text for more details.

Gómez-Valent & de Cruz Pérez 2017c), we find

$$\phi(a) = \left[ \frac{3\alpha(\alpha+2)^2 \kappa M_P^4}{64\pi(\alpha+6)} \rho_r^{-1}(a) \right]^{1/(\alpha+2)}, \quad (6)$$

together with  $\phi'(a)$  obtained from it. Here  $\rho_r$  is the radiation energy density, which includes the (massive) neutrino contribution. These initial conditions are used for the numerical solution at any subsequent epoch.

To compare the theoretical predictions of the different models under study with the available observational data we have made use of the Boltzmann code CLASS in combination with the powerful MCMC sampler MontePython (Blas et al., Audren et al. 2011,2013). In the particular instance of  $\phi$ CDM we have modified CLASS such as to implement the shooting method (Stoer & Bulirsch 2010), what allowed us to consistently determine the value of  $\kappa$  for each value of the free parameter  $H_0$ . As it is well-known, such numerical technique consists in replacing a boundary value problem with an initial value one through a large number of iterations of the initial conditions until finding the optimized solution. For the  $\phi$ CDM, the initial conditions are determined by (6) and its time derivative, which are both explicitly dependent on  $\kappa$ .

### 3. DATA

To generate the fitting results displayed in Tables 1 and 2 we have run the MCMC code MontePython, together with CLASS, over an updated data set SNIa+ $H(z)$ +BAO+LSS+CMB, consisting of: i) 6 effective points on the Hubble rate from the Pantheon+MCT sample (Scolnic et al., Riess et al. 2018,2018b), which includes 1063 SNIa; ii) 31 data from  $H(z)$  from cosmic chronometers (Jimenez et al. 2003; Simon et al. 2005; Stern et al. 2010; Moresco et al. 2012,2015,2016; Zhang et al. 2014; Ratsimbazafy 2017); iii) 16 effective BAO points (Kazin et al. 2014; Gil-Marín et al. 2016; Bourboux et al. 2017; Carter et al. 2018; Gil-Marín et al. 2018); iv) 19 effective points from LSS, specifically 18 points from the observable  $f(z)\sigma_8(z)$  (mostly RSD) (Guzzo et al., Song & Percival 2008,2009; Blake et al. 2011,2013; Beutler et al. 2012; Okumura et al. 2016; Gil-Marín et al. 2016; Simpson et al. 2016; Howlett et al. 2017; Shi et al. 2018;

Gil-Marín et al. 2018; Mohammad et al. 2018) and an effective one from the Weak Lensing (WL) observable  $S_8 \equiv \sigma_8(0) \left(\frac{\Omega_m}{0.3}\right)^{0.5}$  (Hildebrandt et al. 2017); v) Finally we make use of the full CMB likelihood from Planck 2015 TT+lowP+lensing (Planck Collab. 2015).

The total data set just described will be referred to as DS1. For a more detailed discussion of these data, see (Solà, Gómez-Valent & de Cruz Pérez 2017a,b). In this study, however, we wish to isolate the effect from the triad of data components BAO+LSS+CMB. These ingredients may be particularly sensitive to the DDE, as shown in the previous references. Such subset of DS1 will be called DS2 and contains the same data as DS1 except SNIa+ $H(z)$ . In the next section we define further specifications of these two datasets with special properties.

### 4. SPECTRUM VERSUS BISPECTRUM

The usual analyses of structure formation data in the literature are performed in terms of the matter power spectrum  $P(\mathbf{k})$ , referred to here simply as spectrum. As we know, the latter is defined in terms of the two-point correlator of the density field  $D(\mathbf{k})$  in Fourier space, namely  $\langle D(\mathbf{k}) D(\mathbf{k}') \rangle = \delta(\mathbf{k} - \mathbf{k}') P(\mathbf{k})$ , in which  $\delta$  is the Dirac delta of momenta. For a purely Gaussian distribution, any higher order correlator of even order decomposes into sums of products of two-point functions, in a manner very similar to Wick's theorem in QFT. At the same time, all correlators of odd order vanish. This ceases to be true for non-Gaussian distributions, and the first nonvanishing correlator is then the bispectrum  $B(\mathbf{k}_1, \mathbf{k}_2, \mathbf{k}_3)$ , which is formally connected to the three-point function

$$\langle D(\mathbf{k}_1) D(\mathbf{k}_2) D(\mathbf{k}_3) \rangle = \delta(\mathbf{k}_1 + \mathbf{k}_2 + \mathbf{k}_3) B(\mathbf{k}_1, \mathbf{k}_2, \mathbf{k}_3). \quad (7)$$

The Dirac  $\delta$  selects in this case all the triangular configurations. Let us note that even if the primeval spectrum would be purely Gaussian, gravity makes fluctuations evolve non-Gaussian. Therefore, such deviations with respect to a normal distribution may be due both to the evolution of gravitational instabilities that are amplified from the initial perturbations, or even from some intrinsic non-Gaussianity of the primordial spectrum.

The bispectrum (BSP) has been described in many places in the literature, see e.g. Amendola & Tsujikawa,

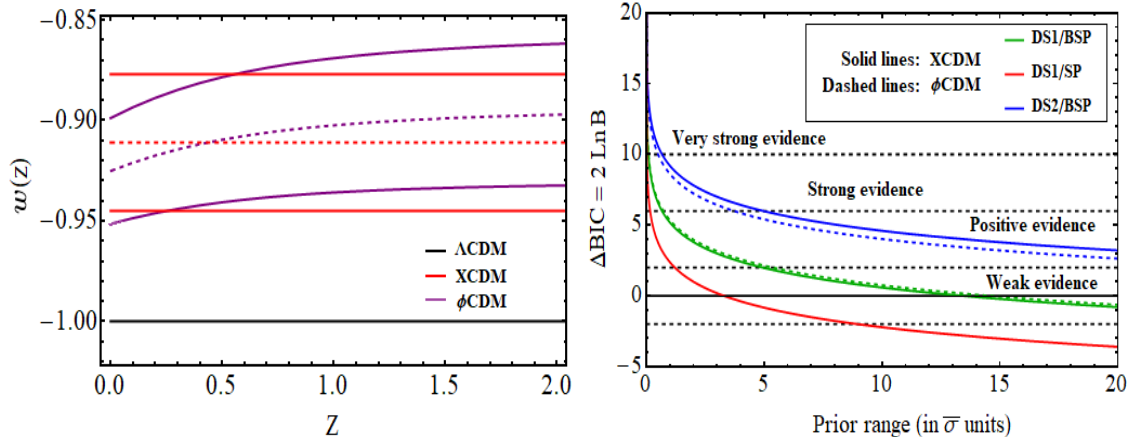


FIG. 2.— (Left) The EoS for the DE models within the corresponding  $1\sigma$  bands and under scenario DS2/BSP. For the XCDM the EoS is constant and points to quintessence at  $\sim 2.6\sigma$  c.l. (cf. Table 2). For the  $\phi$ CDM the EoS evolves with time and is computed through a Monte Carlo analysis. The current value is  $w(z=0) = -0.925 \pm 0.026$  and favors once more quintessence at  $\sim 2.9\sigma$  c.l.; (Right) The full Bayesian evidence curves for the various models as compared to the  $\Lambda$ CDM as a function of the prior range (in  $\bar{\sigma}$  units, see text).

Liddle & Lyth (2009,2010) and references therein. Here we wish to dwell on its impact as a potential tracer of the DDE. Observationally, the data on BAO+LSS (more specifically, the  $f\sigma_8$  part of LSS) including both the spectrum (SP) and bispectrum (BSP) are taken from (Gil-Marín et al. 2016), including the correlations among these data encoded in the provided covariance matrices. The same data including SP but no BSP has been considered in (Alam et al. 2017). In this study, we analyze the full dataset DS1 with spectrum only (dubbed DS1/SP) and also the same data when we include both SP and BSP (denoted DS1/BSP for short). In addition, we test the DDE sensitivity of the special subset DS2 including both SP+BSP components (scenario DS2/BSP). Other combinations will be presented elsewhere in an extended study. The corresponding fitting results are displayed in Tables 1 and 2. While we use Planck 2015 CMB data with full likelihood throughout most of our analysis, in the second block of Table 2 we report on the preliminary results obtained from the recent Planck 2018 CMB data under compressed likelihood (Chen, Huang & Wang, Planck Collab. 2018). The full likelihood for Planck 2018 CMB data is not public yet.

## 5. CONFRONTING DDE TO OBSERVATIONS

As we can see from Tables 1 and 2, the comparison of the  $\Lambda$ CDM with the DDE models depends on the data sets used. If we focus on DS1/SP there is no evidence that the DDE models perform better than the  $\Lambda$ CDM. For example, the XCDM yields a weak signal which is compatible with  $w_0 = -1$  (i.e. a rigid CC). This is consistent e.g. with the analysis of Park & Ratra (2018a). The  $\phi$ CDM model remains also inconclusive under the same data. The upper bound of  $\alpha < 0.092$  at  $1\sigma$  ( $< 0.178$  at  $2\sigma$ ) is consistent, too, with previous studies (Park & Ratra 2018b). However, both the XCDM parametrization and the  $\phi$ CDM model are able to fare better than the  $\Lambda$ CDM if we consider the dataset DS1/BSP, i.e. upon including the bispectrum component of the BAO+LSS data. The DDE signal is maximized within the restricted DS2/BSP dataset, where

both the XCDM and the  $\phi$ CDM reach more than  $2.5\sigma$  c.l. (cf. Table 2). As for the CPL parametrization (1), we do not record it explicitly in the tables, but we have checked that using DS1/BSP the errors in the EoS parameters are still too big to capture any clear sign of DE dynamics. Specifically, we find  $w_0 = -0.934^{+0.067}_{-0.075}$  and  $w_1 = -0.045^{+0.273}_{-0.204}$ , hence fully compatible with a rigid CC ( $w_0 = -1, w_1 = 0$ ). The large size of the errors is due to having one more parameter here. We shall not consider the CPL any longer in our considerations.

In Fig. 1 we display the contour plots for the XCDM and  $\phi$ CDM models at different confidence levels. The EoS parameter  $w_0$  of the XCDM is seen to be shifted upwards more than  $2.5\sigma$  away from  $-1$  and hence it lies in the quintessence region. In the  $\phi$ CDM case we consistently find  $\alpha > 0$  at a similar c.l. In Fig. 2 (left) we plot the EoS of the various models in terms of the redshift near our time, including the  $1\sigma$  error bands for the XCDM and  $\phi$ CDM. The latter have been computed from a Monte Carlo analysis sampling the  $w(z)$  distributions. The behavior of the curves shows that the quintessence-like behavior is sustained until the present epoch. For the  $\phi$ CDM  $w(z=0) = -0.925 \pm 0.026$ , thus implying DDE at a c.l. near  $\sim 2.9\sigma$ , which is consistent with the XCDM result.

Finally, in Fig. 3 we compute the matter power spectrum and the temperature anisotropies for the DDE models using Planck 2015 data, and also display the percentage differences with respect to the  $\Lambda$ CDM. The CMB anisotropies remain safely of order  $\sim 1\%$  at most for the entire range.

## 6. DISCUSSION

The main results of this work are synthesized in our tables and figures. As pointed out before, in the absence of BSP data the DDE signs are weak and we find consistency with previous studies. However, when we include BSP data and focus on the LSS+BAO+CMB observables (i.e. scenario DS2/BSP) the situation changes. Both models XCDM and  $\phi$ CDM consistently point to a

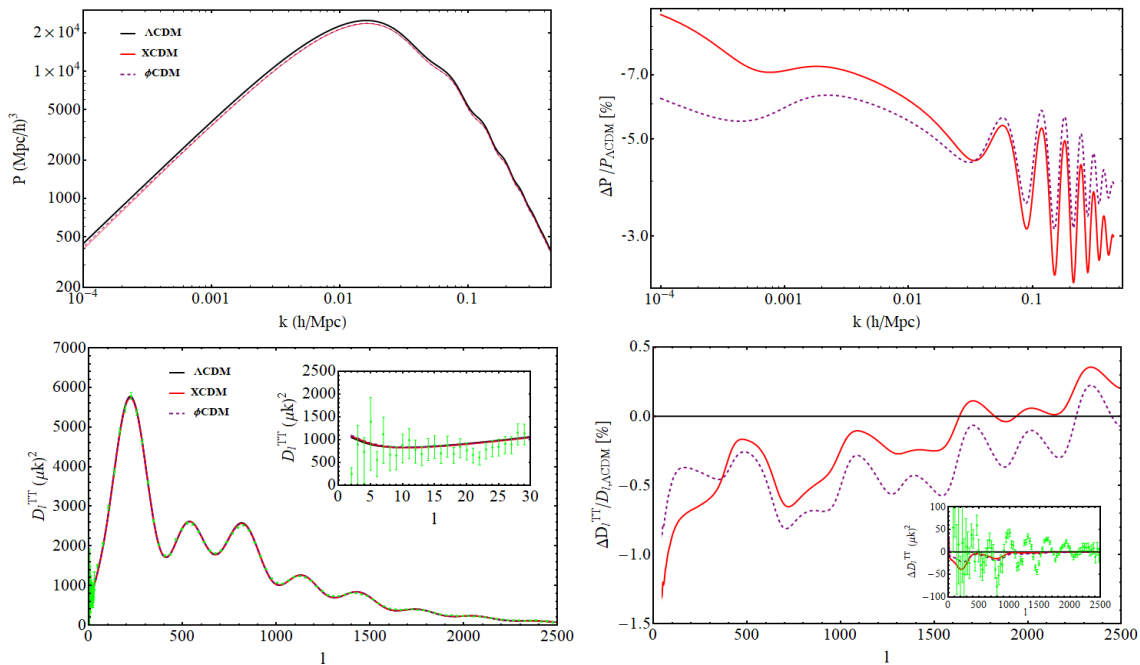


FIG. 3.— (Upper plots) The power spectrum for the DDE models under consideration side by side with the relative (percentage) differences with respect to that of the  $\Lambda$ CDM; (Bottom plots) As before, but considering the CMB temperature anisotropies for Planck 2015 data. The inner plots show additional details including the data points with the corresponding errors in part or the whole available angular range.

$> 2.5\sigma$  effect. Specifically, the evolving EoS of the  $\phi$ CDM takes a value at present which lies  $\sim 2.9\sigma$  away from the  $\Lambda$ CDM case ( $w = -1$ ) into the quintessence region (cf. Fig. 2, left). The significance of these effects can be further appraised by computing the full Bayesian evidence curves, see Fig. 2 (right), as a function of the prior range. We use  $\bar{\sigma}$  as a unit of measure of such range, defining  $\bar{\sigma}$  as half the sum of the upper and lower fitting errors of the DDE parameters in the tables. Specifically, we plot  $\Delta\text{BIC} \equiv 2 \ln B$ , i.e. twice the log of the Bayes factor (viz. the ratio of marginal likelihoods of the DDE models and the  $\Lambda$ CDM). The ranges of values of  $\Delta\text{BIC}$  corresponding to very strong, strong, moderate or weak evidence (Kass & Raftery 1995) are explicitly shown in Fig. 2 (right).

We have used the code MCEvidence (Heavens et al. 2017) to compute  $\Delta\text{BIC}$ , and we have compared the results with the (analytic expression) for Gaussian distributions, the two results being qualitatively similar but with some numerical differences that we will disclose elsewhere. From the exact curves in Fig. 2, obtained with MCEvidence, we reconfirm that with the dataset involving only the power spectrum the evidence is weak. But at the same time we can see that both for the XCDM and  $\phi$ CDM there appears strong evidence of DDE within scenario DS2/BSP up to  $5\bar{\sigma}$ , with a long tail of moderate positive evidence up to more than  $20\bar{\sigma}$ . Incidentally, these evidence results resemble those reported sometime ago in (Salvatelli et al. 2014), but for very different models and for older (Planck2013+WMAP) data, and with no inclusion of BSP (not available at that time). The fact that with the Planck 2015 data and with tra-

ditional models and parametrizations of the DE we can still reach such significant level of evidence is encouraging. Even more reassuring is the fact that with the preliminary Planck 2018 data we can reach similar levels of evidence (cf. Table 2, second block), which will have to be confirmed when the full Planck 2018 likelihood will be made public.

Let us finally note that, in the presence of BSP data, the values of  $\sigma_8(0)$  shown in the tables (specially in Table 2) are smaller for the DDE models than for the  $\Lambda$ CDM, what contributes to alleviate the  $\sigma_8(0)$ -tension (Macaulay et al. 2013). We have checked that a similar effect is possible within the  $\Lambda$ CDM (under DS1/BSP) for a sum of neutrinos masses of  $\sum m_\nu = 0.195 \pm 0.076$  eV, leading to  $\sigma_8(0) = 0.785 \pm 0.014$ , which is however unfavored by the usual constraints on neutrino oscillations since it requires unnatural fine-tuning.

To summarize, our study shows that it is possible to reach significant signs of DDE with the current data, provided we use the bispectrum in combination with the power spectrum. The former might be a good tracer of dynamical DE effects and ultimately of the “fine structure” of the DE. The details of this analysis will be presented elsewhere.

## 7. ACKNOWLEDGEMENTS

We are funded by projects FPA2016-76005-C2-1-P (MINECO), 2017-SGR-929 (Generalitat de Catalunya) and MDM-2014-0369 (ICCUB). JdCP also by a FPI fellowship associated to FPA2016. We are thankful to Y. Fantaye for support in the use of package MCEvidence.

## REFERENCES

Alam, S., et al. 2017, MNRAS, **470**, 2617.

Amendola, L. & Tsujikawa, S. 2010, *Dark Energy* (Cambridge Univ. Press); Liddle, A.R. & Lyth, D.H. 2009, *The Primordial Density Perturbation* (Cambridge Univ. Press).

- Beutler, F., *et al.* 2012, MNRAS, **423**, 3430.
- Blake, C., *et al.* 2011, MNRAS, **415**, 2876; Blake, C., *et al.* 2013, MNRAS, **436**, 3089.
- Blas, D., Lesgourgues, J. & Tram, T. 2011, JCAP, **1107**, 034;
- Audren, B., Lesgourgues, J. & Benabed, K. 2013, JCAP, **1302**, 001.
- Bourboux, H.D.M.D., *et al.* 2017, Astron. Astrophys., **608**, A130.
- Carter, P., *et al.* 2018, MNRAS, **481**, 2371.
- Chen, L., Huang, Q.-G. & Wang, K. 2018, arXiv:1808.05724;
- Planck Collab. 2018, Aghanim, N., *et al.* 2018, arXiv:1807.06209.
- Chevallier, M. & Polarski, D., 2001, Int. J. Mod. Phys. D, **10**, 213; Linder, E.V., 2003, Phys. Rev. Lett., **90**, 091301.
- Costa, A.A., Xu, X-D., Wang, B. & Abdalla, E. 2017, JCAP, **1701**, 028.
- Ferreira, E.G.M., *et al.* 2017, Phys. Rev. D, **95**, 043520.
- Gil-Marín, H., *et al.* 2016, MNRAS, **465**, 1757.
- Gil-Marín, H., *et al.* 2018, MNRAS, **477**, 1604.
- Guzzo, L., *et al.* 2008, Nature, **451**, 541; Song, Y-S. & Percival, W.J. 2009, JCAP, **10**, 004.
- Heavens, A., Fantaye, Y., Mootoooloo, A., *et al.* 2017, arXiv:1704.03472.
- Hildebrandt, H., *et al.* 2017, MNRAS, **465**, 1454.
- Howlett, C., *et al.* 2017, MNRAS, **471**, 3135.
- Jiménez, R., Verde, L., Treu, T. & Stern, D. 2003, ApJ, **593**, 622.
- Kass, R.E. & Raftery, A. 1995, J. Amer. Statist. Assoc., **90**, 773.
- Kazin, E.A., *et al.* 2014, MNRAS, **441**, 3524.
- Macaulay, E., Wehus, I.K. & Eriksen, H.C. 2013, Phys. Rev. Lett., **111**, 16130.
- Mohammad, F.G., *et al.* 2018, Astron. Astrophys., **619**, A17.
- Moresco, M., *et al.* 2012, JCAP, **1208**, 006; Moresco, M. 2015, MNRAS, **450**, L16; Moresco, M., *et al.* 2016, JCAP, **1605**, 014.
- Okumura, T., *et al.* 2016, Publ. Astron. Soc. Jap., **68**, 38.
- Park, C-G. & Ratra, B. 2018a, arXiv:1803.05522.
- Park, C-G. & Ratra, B. 2018b, arXiv:1807.07421.
- Peebles, P.J.E. & Ratra, B. 1988, ApJ, **325**, L17; Ratra, B. & Peebles, P.J.E. 1988, Phys. Rev. D, **37**, 3406.
- Peebles P.J.E. & Ratra, B. 2003, Rev. Mod. Phys., **75** 559;
- Padmanabhan, T. 2003, Phys. Rept., **380**, 235.
- Planck Collab. 2015, Ade, P.A.R., *et al.* 2016, Astron. Astrophys., **594**, A13;
- Ratsimbazafy, A.L., *et al.* 2017, MNRAS, **467**, 3239.
- Riess, A.G., *et al.* 1998, ApJ, **116**, 1009; Perlmutter, S., *et al.* 1999, ApJ, **517**, 565.
- Riess, A.G., *et al.* 2016, ApJ, **826**, 56; Riess, A.G., *et al.* 2018a, ApJ, **855**, 136.
- Salvatelli, V., *et al.* 2014, Phys. Rev. Lett., **113**, 181301.
- Scolnic, D.M., *et al.* 2018, ApJ, **859**, 101; Riess, A.G., *et al.* 2018b, ApJ, **853**, 126.
- Shi, F., *et al.* 2018, ApJ, **861**, 137.
- Simon, J., Verde, L. & Jiménez, R. 2005, Phys. Rev. D, **71**, 123001.
- Simpson, F., *et al.* 2016, Phys. Rev. D, **93**, 023525.
- Solà, J. 2013, J. Phys. Conf. Ser., **453**, 012015.
- Solà, J., Gómez-Valent, A. & de Cruz Pérez, J. 2015, ApJ, **811**, L14.
- Solà, J., Gómez-Valent A. & de Cruz Pérez, J. 2017a, ApJ, **836**, 43.
- Solà, J., Gómez-Valent A. & de Cruz Pérez, J. 2017b, Phys. Lett. B **774**, 317; 2018a, EPL, **121**, 39001; 2018b, MNRAS, **478**, 4357.
- Solà, J., Gómez-Valent A. & de Cruz Pérez, J. 2017c, Mod. Phys. Lett. A, **32**, 1750054.
- Stern, D., *et al.* 2010, JCAP, **1002**, 008.
- Stoer, J. & Bulirsch, R. 2010, *Introduction to Numerical Analysis* (New York: Springer).
- Tsiapi, P. & Basilakos, S. 2018, arXiv:1810.12902.
- Turner, S.M. & White, M. 1997, Phys. Rev. D, **56**, R4439.
- Valentino, E.D., Melchiorri, A. & Mena, O. 2017, Phys. Rev. D, **96**, 043503.
- Weinberg, S. 1989, Rev. Mod. Phys., **61**, 1.
- Zhang, C., *et al.* 2014, Res. Astron. Astrophys., **14**, 1221.
- Zhao, G.B., *et al.* 2017, Nat. Astron., **1**, 627.